Inorganic Chemistry

pubs.acs.org/IC Article

Electron-Precise Semiconducting $ReGa_2Ge$: Extending the $IrIn_3$ Structure Type to Group 7 of the Periodic Table

Maxim S. Likhanov, Valeriy Yu. Verchenko, Andrei A. Gippius, Sergei V. Zhurenko, Alexey V. Tkachev, Zheng Wei, Evgeny V. Dikarev, Alexey N. Kuznetsov, and Andrei V. Shevelkov*

Cite This: *Inorg. Chem.* 2020, 59, 12748–12757 Read Online

ACCESS | Metrics & More | Article Recommendations | Supporting Information

ABSTRACT: Intermetallic compounds with semiconducting properties are rare, but they give rise to advanced materials for energy conversion and saving applications. Here, we present $ReGa_2Ge$, a new electron-precise narrow-gap intermetallic semiconductor. The compound crystallizes in the $IrIn_3$ structure type (space group $P4_2/mnm$, a = 6.5734(3) Å, c = 6.7450(8) Å, and Z = 4), where Re atoms occupy the Ir site, while Ga and Ge jointly populate the In sites. ^{69,71}Ga nuclear quadrupole resonance spectroscopy indicates nonstatistical partially ordered distribution of Ga and Ge over two available crystallographic sites; however, the Ga:Ge ratio is exactly 2:1 without noticeable homogeneity range. The stoichiometry of $ReGa_2Ge$ ensures its precise valence electron count, which is 17 e^- per formula unit. Accordingly, a narrow energy gap opens up at the Fermi energy in the electronic structure. Electrical resistivity, Seebeck coefficient, and thermal conductivity are in agreement with the semiconducting behavior deduced from the electronic structure calculations and point to prospective thermoelectric properties at high temperatures. Bonding analysis reveals dominant covalency in Re−E (E = Ga, Ge) and Re−Re interactions.

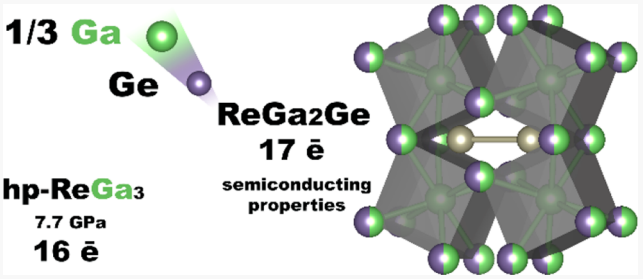

INTRODUCTION

Intermetallic compounds with semiconducting properties are rare, but they exhibit peculiar chemical bonding and promising functional properties.[1,2] In the first place, intermetallic narrow-gap semiconductors give rise to advanced thermoelectric materials with high efficiency of energy conversion.[2−7] The number of semiconducting intermetallic compounds is not large: most representatives are found in the limited number of structure types, although there are individual representatives, too. Opening of the energy gap in intermetallic compounds generally takes place as a result of hybridization of valence orbitals, when two or more metals from different blocks of the Periodic Table are involved in chemical bonding. Thus, one can distinguish three major families containing semiconducting intermetallic compounds. Those are Heusler compounds,[8−11] Nowotny chimney-ladder phases,[12−14] and $IrIn_3$-type compounds.[15] Among Heusler compounds, the MgAgAs-type representatives (half-Heusler alloys) composed of main group elements show large energy gaps. At the same time, the Nowotny chimney ladders and $IrIn_3$-type intermetallics contain metals of the d- and p-blocks, and possess narrow energy gaps.

The $IrIn_3$ structure type includes 10 individual binary compounds that exist under normal conditions. They are $FeGa_3$, $CoGa_3$, $CoIn_3$, $RuGa_3$, $RuIn_3$, $RhGa_3$, $RhIn_3$, $OsGa_3$, $IrGa_3$, and $IrIn_3$.[15−21] Notably, these compounds are formed exclusively between d-metals of the groups 8 and 9 and gallium or indium. The crystal structure is relatively simple as shown in Figure 1. The p-element (p-M2) forms the framework of the structure, where two types of voids are present. The cubic voids are centered by p-metal atoms (p-M1), whereas the rhombic prisms are occupied by transition-metal atom dumbbells (d-M).

Among all representatives, only compounds having the valence electron count (VEC) of 17 ($FeGa_3$, $RuGa_3$, $OsGa_3$, and $RuIn_3$[15−20]) are semiconductors, while the remaining 18-

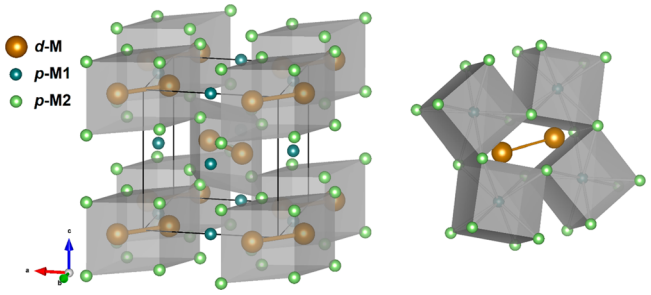

Figure 1. Crystal structure of the $IrIn_3$ type: a unit cell in the polyhedral representation (left) and a dumbbell of transition metal atoms in the environment of p-M1@p-$M2_8$ cubes (right).

Received: June 18, 2020
Published: August 26, 2020

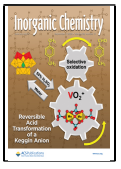

https://dx.doi.org/10.1021/acs.inorgchem.0c01805
Inorg. Chem. 2020, 59, 12748−12757

electron compounds ($CoGa_3$, $RhGa_3$, $IrGa_3$, $CoIn_3$, $RhIn_3$, and $IrIn_3$[15,16,19,21,22]) are metallic conductors. The only example of the 16-electron phase is $ReGa_3$;[23] however, this compound is formed under high pressure (7.7 GPa) and high temperature (1000 K), and decomposes under normal conditions.

In this work, a new member of the $IrIn_3$ structure type, $ReGa_2Ge$, composed of the group 7 transition metal rhenium and a combination of gallium and germanium was synthesized. The combination of gallium and germanium pursues two goals. First, it provides the chemical pressure through the substitution of gallium by slightly smaller germanium, similar to the physical pressure, which was used to synthesize $ReGa_3$.[23] Second, the aliovalent substitution of germanium for gallium allows movement from the unstable 16-electron configuration of $ReGa_3$ to the persistent and stable 17-electron one in $ReGa_2Ge$. This composition was chosen as a starting point of our research. The $ReGa_2Ge$ compound, as expected, possesses nonmetallic properties, which are confirmed by the electronic structure calculations and by the experimental study of transport properties.

EXPERIMENTAL SECTION

Synthesis and Characterization. Synthesis of polycrystalline samples of $ReGa_{2+x}Ge_{1-x}$ (x from −0.04 to 0.04 with the step of 0.01) was carried out by the standard ampule technique using rhenium powder (99.99%, Sigma-Aldrich), germanium chips (99.999%, Sigma-Aldrich), and gallium ingots (99.9999%, Sigma-Aldrich). Evacuated (residual pressure of 1×10^{-3} Torr) and sealed quartz ampules with a mixture of metals in the desired stoichiometric ratio were annealed at 950 °C for 2 days. After that, the samples were ground into powders, pressed into pellets, and annealed at 750 °C for 1 week.

Single crystals of $ReGa_2Ge$ were grown using chemical transport reactions. For this, the presynthesized single-phase powder of $ReGa_2Ge$ (0.3 g) was loaded into a quartz ampule together with several crystals of I_2 (~3 mg) as a transport agent. The ampule with an inner diameter of 0.8 and 10 cm in length was evacuated, sealed off, and annealed in a two-zone horizontal furnace having a temperature gradient along the tube. The load temperature was 750 °C, while the crystallization zone was kept at 700 °C for 10 days. As a result, small needle-like crystals were obtained with the composition of $Re_{1.01(2)}Ga_{1.99(2)}Ge_{1.00(2)}$ according to the energy-dispersive X-ray spectroscopy (EDXs). At the same time, chemical transport starting from the stoichiometric mixture of elements was not successful.

Powder X-ray diffraction (PXRD) analysis was performed using a Huber G670 Guinier Camera (Cu Kα_1 radiation, Ge monochromator, λ = 1.5406 Å). The data were collected by scanning the image plate four times after an exposure time of 2400 s at room temperature.

A scanning electron microscope JSM JEOL 6490-LV equipped with an energy dispersive X-ray (EDX) analysis system INCA x-Sight was used for the analysis of chemical composition. For this, three $ReGa_{2+x}Ge_{1-x}$ samples with x = −0.04, 0, and 0.04 were finely ground and pressed into pellets.

The melting point of $ReGa_2Ge$ was determined by differential scanning calorimetry with a heating rate of 10 K/min in the temperature range of 300−1300 K in an argon atmosphere using a STA 409 PC Luxx thermal analyzer (Netzsch).

The ^{69,71}Ga nuclear quadrupole resonance (NQR) measurements were performed at 77 K utilizing a home-built phase coherent pulsed NQR spectrometer with direct digital quadrature detection at the carrier frequency. The ^{69,71}Ga NQR spectra were measured using a frequency step point-by-point spin−echo technique. At each frequency point, the area under the spin−echo magnitude was integrated in the time domain and averaged by a number of accumulations, which depends on the Ga isotope and frequency. Alternatively, we used a Fourier transform summation (FTS) method for spectra accumulation since the ^{69,71}Ga NQR lines are rather broad.[24]

Crystal Structure Determination. Single crystals of $ReGa_2Ge$ were investigated at 100(2) K on a Bruker D8 VENTURE single-crystal X-ray diffractometer equipped with PHOTON 100 CMOS detector, graphite monochromator, and Mo-target X-ray tube (λ = 0.73071 Å). The frame width of 0.50° and exposure time of 15 s/frame were employed for data collection. Data reduction and integration were performed with the Bruker software package SAINT (Version 8.38A).[25] The absorption correction was performed using the multiscan routine as implemented in SADABS (Version 2014/5).[26,27] The crystal structure was solved by the charge-flipping algorithm and refined against $|F^2|$ in the full-matrix anisotropic approximation using the Jana2006 program.[28] Occupancies of the p-element positions containing gallium and germanium atoms were fixed according to the nominal composition of $ReGa_2Ge$.

For the single-phase polycrystalline sample of $ReGa_2Ge$, the crystal structure was refined using the Rietveld method in the Jana2006 program.[28]

Crystallographic data as well as structure solution and refinement details are presented in Tables 1 and 2 for the single-crystal X-ray diffraction experiment. Crystallographic data obtained for the $ReGa_2Ge$ polycrystalline sample are shown in the Supporting Information.

Electronic Structure Calculations. The atomic coordinates and unit cell parameters obtained from the single-crystal X-ray diffraction experiment were used for electronic structure calculations within the density functional theory (DFT) approach using the Full-Potential Local-Orbital minimum basis band-structure (FPLO) code (version 14.00−47).[29] The local density approximation (LDA) functional was used to treat the exchange-correlation energy in the fully relativistic regime.[30] Band structure calculations were performed using three models:

- Model A. Statistical distribution of gallium and germanium over the E1 and E2 sites, with the occupancy ratio of 1:2 for each E position.
- Model B. Occupation of the E1 and E2 sites by gallium and germanium according to the multiplicity of sites and stoichiometry of the metals. In this case, gallium atoms occupy the E2 site, whereas germanium atoms populate the E1 site.
- Model C. Occupation of the E1 site by gallium, and the E2 site jointly by gallium and germanium in the 1:1 ratio. In the cases of Model A and Model C, the band structures were calculated

Table 1. Crystallographic Data and Refinement Parameters for $ReGa_2Ge$ from the Single-Crystal X-ray Diffraction

formula	$ReGa_2Ge$
formula weight (g·mol^{-1})	398.20
crystal system	tetragonal
space group	$P4_2/mnm$
a (Å)	6.5734(3)
c (Å)	6.7450(8)
V (Å^3)	291.45(4)
Z	4
ρ_{calc} (g·cm^{-3})	9.076
μ, mm^{-1}	69.556
temperature (K)	100
radiation, λ (Å)	Mo Kα, 0.71073
absorption correction	Multi-scan
θ range (deg)	4.33−38.56
index ranges	$-11 \le h \le 11$
	$-11 \le k \le 11$
	$-11 \le l \le 11$
N collected	10841
N unique/N observed [$I > 2\sigma(I)$]	482/482
R_1 [$I > 2\sigma(I)$]	0.0311
wR_2 [$I > 2\sigma(I)$]	0.0358
GOF	1.72

https://dx.doi.org/10.1021/acs.inorgchem.0c01805
Inorg. Chem. 2020, 59, 12748−12757

Table 2. Atomic Coordinates and Thermal Displacement Parameters for the Crystal Structure of $ReGa_2Ge$

atom	Wyckoff site	x	y	z	U_{eq}, Å^2	occupancy
Re1	4*f*	0.34104(5)	0.34104(5)	0	0.00329(9)	1
E1	4*c*	0	0.5	0	0.0055(3)	2/3Ga + 1/3Ge[a]
E2	8*j*	0.15555(10)	0.15555(10)	0.26561(13)	0.0034(2)	2/3Ga + 1/3Ge[a]

[a]Fixed according to the sample composition.

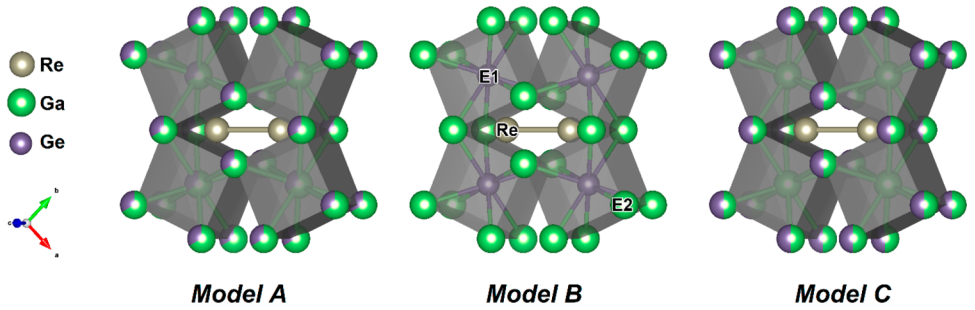

Figure 2. Distribution of gallium and germanium atoms over the E1 and E2 sites according to Models A−C. Re is shown in gray, Ga in green, and Ge in purple.

within the virtual crystal approximation (VCA), where the mean nuclear charge of 31.33 (the E1 and E2 sites for Model A) or 31.5 (the E2 site for Model C) was used, and the number of electrons in the system was changed accordingly in the exchange-correlation potential. Integrations in the k-space were performed by an improved tetrahedron method[31] on a grid of 16 × 16 × 16 k-points. All models are compared in Figure 2.

Bonding Analysis. Chemical bonding analysis was performed via studying the QTAIM charge density and electron localization function (ELF) topology for the ordered structure model (Model B) obtained based on the DFT calculations using the projector augmented wave method (PAW) as implemented in the Vienna Ab initio simulation package (VASP).[32,33] The Perdew−Burke−Ernzerhof exchange-correlation functional (PBE)[34] of the GGA type was used for the calculations, with a Brillouin zone sampling using a Monkhorst−Pack[35] grid of 12 × 12 × 12 k-points. Energy cutoff was set to 500 eV, and the energy convergence criterion was at 10^{-5} eV. Convergence toward the k-point set and energy was checked. Topological analysis of charge density and ELF was performed using Multiwfn 3.7 package.[36] ELF was visualized using VESTA 3 package.[37]

Transport Properties. Electrical resistivity, Seebeck coefficient, and thermal conductivity were measured on a rectangular-shaped sample with the dimensions of 8 × 3 × 2 mm^3 using the resistivity and thermal transport options of a Physical Property Measurement System (PPMS, Quantum Design) in the temperature range of 2−400 K. All measurements were carried out in a zero magnetic field. Pellets were pressed from the $ReGa_2Ge$ powdered sample at the external pressure of ∼100 bar at room temperature. The density of the pellet was ∼88% of the theoretical value based on the determined mass and linear sizes.

RESULTS AND DISCUSSION

Synthesis, Crystal Structure, and Homogeneity Range. Synthesis of the $ReGa_{2+x}Ge_{1-x}$ samples (x from −0.04 to 0.04) was carried out in two stages: the first one included annealing at 950 °C, and the second at 750 °C. The initial high-temperature annealing is necessary because no ternary compounds were observed after the midtemperature heating (for example, at 750 °C) according to PXRD analysis. These samples were found to contain unreacted starting materials together with minor admixtures of Re_3Ge_7 and $ReGa_5$.[38,39] Apparently, this fact is associated with the kinetic inertness of the starting materials with respect to each other, and the high-temperature annealing increases the reactivity, thus ensuring the chemical reaction.

According to the combination of the DSC and PXRD analysis, $ReGa_2Ge$ melts incongruently at 800(10) °C, yielding $ReGa_{0.4}Ge_{0.6}$,[40] $ReGaGe_2$, and the high-temperature melt.

All reflections on the PXRD pattern of the sample with the stoichiometric composition of $ReGa_2Ge$ were indexed in the tetragonal crystal system with the unit cell parameters close to those of $ReGa_3$.[23] No impurities were observed. The $ReGa_2Ge$ powder was used for growing single crystals in the temperature gradient of 750−700 °C using iodine as a transport agent.

The crystal structure solution and refinement have shown that $ReGa_2Ge$ crystallizes in the $IrIn_3$ structure type (space group $P4_2/mnm$). The Rietveld refinement against the PXRD data demonstrates the same result. All interatomic distances are in the range typical for the $IrIn_3$-type representatives. For example, the Re−Re distance (2.96 Å) is comparable with other distances within the dumbbells of transition metals in isomorphous $RuGa_3$ (2.91 Å),[15] $RuIn_3$ (3.07 Å),[41] $RhIn_3$ (3.04 Å),[22] and $IrIn_3$ (3.06 Å).[22] The distance within the Re−Re dumbbell is slightly longer than the distances in metallic rhenium (2.75−2.77 Å)[42] and corresponds to the chemical bond, which will be discussed below. The E−E distances are in the range between 2.89 and 3.58 Å. The shortest distances are the E1−E2 contacts from the center of the cubic void (E1) to its vertices (2.94 and 3.06 Å). The distances between the E2 atoms are noticeably longer (3.16−3.58 Å), with the exception of one short contact (2.89 Å). The selected interatomic distances in $ReGa_2Ge$ are presented in Table 3.

Since the size of gallium and germanium differs slightly, they may replace each other in intermetallic compounds forming extended solid solutions; thus, the $ReGa_{2+x}Ge_{1-x}$ solid solution was proposed. Indeed, the $FeGa_{3-y}Ge_y$ solid solution has the maximum germanium content of $y_{max} \approx 0.4$,[43] which corresponds to the valence electron concentration of ∼17.4. Surprisingly, we confirmed the absence of a detectable homogeneity region for $ReGa_2Ge$. The PXRD patterns of the $ReGa_{2+x}Ge_{1-x}$ samples with $x = -0.04$, 0, and +0.04 are shown in Figure 3. Clearly, increasing of the gallium content leads to the formation of $ReGa_5$ and metallic Re as admixtures visible on the PXRD pattern. Accordingly, the samples with $x > 0$ lie in the

https://dx.doi.org/10.1021/acs.inorgchem.0c01805
Inorg. Chem. 2020, 59, 12748−12757

Table 3. Selected Interatomic Distances (Å) in the Crystal Structure of $ReGa_2Ge$

Re1	Re1 (×1)	2.9554(7)
	E1[a] (×2)	2.4734(4)
	E2 (×2)	2.4866(9)
	E2 (×4)	2.6027(9)
E1	E2 (×4)	2.9448(8)
	E2 (×4)	3.0630(8)
	E1 (×2)	3.3725(5)
E2	E2 (×1)	2.892(1)
	E2 (×1)	3.162(2)
	E2 (×4)	3.5197(10)
	E2 (×1)	3.583(2)

[a]E = 2/3Ga + 1/3Ge.

Re−$ReGa_5$−$ReGa_2Ge$ compositional triangle. The decrease of the gallium content leads to the admixture of $ReGaGe_2$,[44] such that the compositions with $x < 0$ reside on the $ReGa_2Ge$−$ReGaGe_2$ cut. The unit cell parameters of the $ReGa_2Ge$ phase determined for the samples with the nominal composition in the range of $-0.04 \leq x \leq 0.04$ remain unchanged within the accuracy of determination (see inset in Figure 3). The PXRD data are in agreement with EDXs results for the samples with the nominal composition of $ReGa_{2+x}Ge_{1-x}$ ($x = -0.04$, 0, and 0.04), which indicate the stoichiometry of composition of the target product and the presence of impurities for $x = -0.04$ and 0.04 (Supporting Information, Table S3).

Thus, $ReGa_2Ge$ is a line phase with VEC = 17. Although the 17-electron $IrIn_3$-type compounds demonstrate both the increase and decrease of VEC upon substitutions,[43,45−50] we can assume the importance of the electronic factor for the title compound. The absence of the homogeneity range might indicate possible ordering of gallium and germanium on the E1 and E2 sites. However, there are no unambiguous structural data that confirm a predominant population of the E1 and E2 sites in the $IrIn_3$-type compounds. In the $FeGa_{3-y}Al_y$ solid solution, aluminum atoms preferentially occupy the E2 site.[51] On the contrary, for the $IrIn_{3-y}Mg_y$ solid solution, magnesium atoms concentrate on the E1 site, i.e., in slightly distorted cubes of indium atoms.[52] In a similar fashion, Zn substitutes for In or Ga on the E1 site in $CoIn_{3-x}Zn_x$ and $CoGa_{3-x}Zn_x$.[21]

To shed some light on the distribution of gallium and germanium atoms over the E1 and E2 positions, we performed a ^{69,71}Ga NQR study. The NQR signals are rather broad (Figure 4), more than 4 MHz at the baseline, which is about 20 times wider than the corresponding signals recorded for $FeGa_3$.[53] In both ^{69}Ga and ^{71}Ga subspectra, two signals can be observed. For each pair of signals, the ratio of peak frequencies is 1.59−1.60, which nicely corresponds to the quadrupole moments ratio of two gallium isotopes, $^{69}Q/^{71}Q = 1.60$. The signals centered at 43.4/27.3 MHz and 52.3/32.9 MHz for ^{69}Ga/^{71}Ga (Figure 4) can be unambiguously attributed to gallium atoms occupying the E2 and E1 positions, respectively, based on the comparison

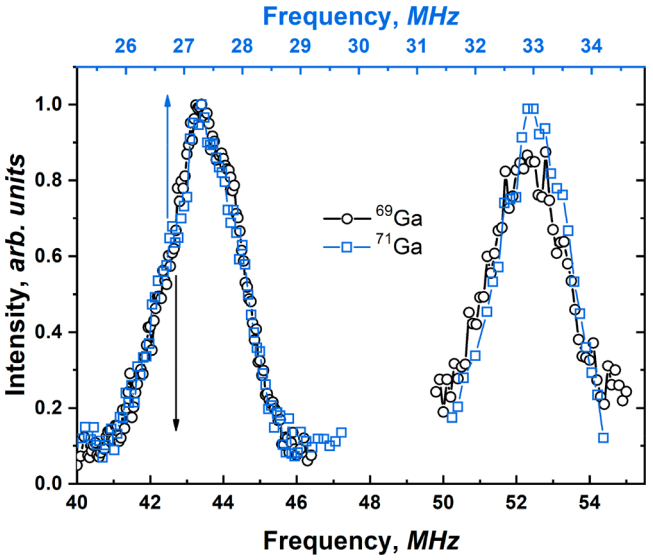

Figure 4. ^{69,71}Ga NQR spectra of $ReGa_2Ge$ measured at 77 K. Frequency scales for two gallium isotopes are related as their quadrupole moments (1.60).

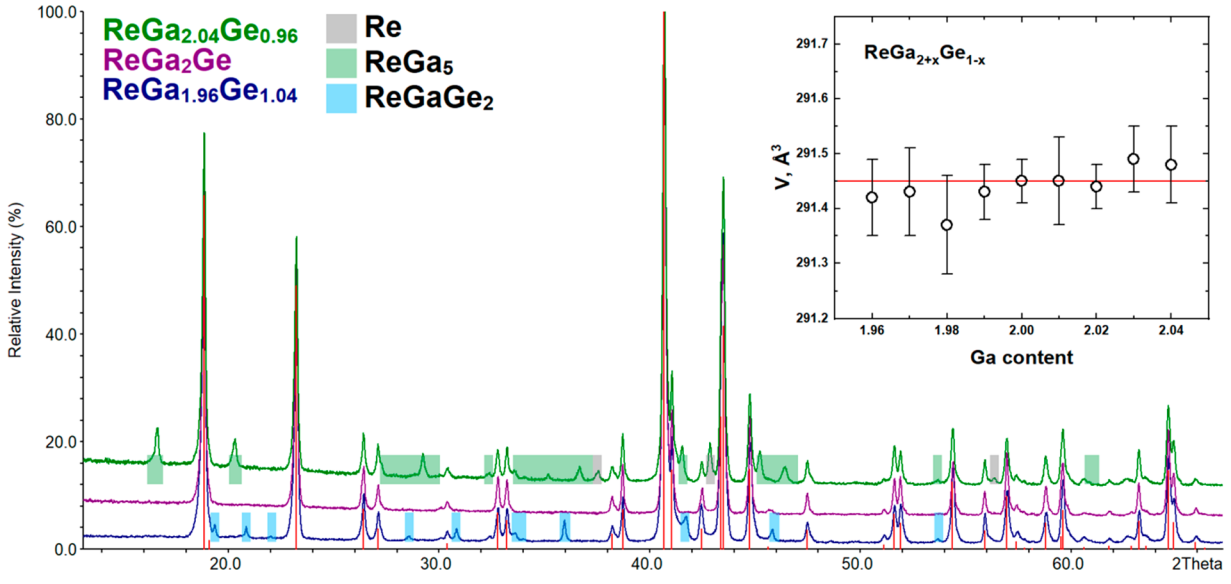

Figure 3. Powder X-ray diffraction patterns of $ReGa_{2+x}Ge_{1-x}$ with $x = -0.04$, 0, and 0.04. Peaks calculated using structural parameters from the single-crystal X-ray diffraction experiment are shown by red lines. Inset: Unit cell volume vs nominal Ga content in $ReGa_{2+x}Ge_{1-x}$.

https://dx.doi.org/10.1021/acs.inorgchem.0c01805
Inorg. Chem. 2020, 59, 12748−12757

with the NQR spectra of $FeGa_3$ and $Fe_{1-x}M_xGa_3$ (M = Co, Re) compounds[48,53,54] and calculated within DFT approximation for $ReGa_3$ (45.9 and 49.1 MHz, respectively).[48]

In order to evaluate the intensity ratio for these two lines, we carefully tuned the experimental conditions for each of them. In particular, the amplitudes of the optimal radio frequency pulses differ by more than 1.5 times. Moreover, the spin−lattice relaxation time T_1 for E1 and E2 sites differs significantly. For example, for ^{69}Ga nuclei T_1(E1) = 0.12(3) s, while T_1(E2) = 3.5(5) s, which makes it necessary to use a rather large repetition period while accumulating data. For both of those sites, relaxation curves are described by a stretched exponent that is characteristic for such wide lines. The resulting integral intensity ratio E2/E1 varies from 0.95(3) for ^{69}Ga to 1.03(3) for ^{71}Ga, which means that gallium atoms occupation numbers for these sites are nearly equal. It can be considered as an argument in favor of Model C with germanium atoms occupying only the E2 site. At the same time, the distribution of Ga and Ge atoms in the latter site seems to be random because of the large width of ^{69,71}Ga NQR lines.

Therefore, the ^{69,71}Ga NQR provides indirect evidence in favor of Model C, although the signal width indicates that no full ordering of Ga and Ge is achieved. Here we note that clusterization of Zn atoms was found in $CoIn_{3-x}Zn_x$ and $CoGa_{3-x}Zn_x$, where X-ray and neutron diffraction studies confirmed at least partial segregation of Zn and Ga/In with concomitant lowering of the crystal symmetry from $P4_2/mnm$ to $P4_2$.[21] However, in the X-ray diffraction experiments, no indications for symmetry lowering due to the close atomic numbers of Ga and Ge were found, probably because in $CoIn_{3-x}Zn_x$ and $CoGa_{3-x}Zn_x$ the Zn atoms are segregated on the E1 site, whereas in $ReGa_2Ge$ we expect at least partial ordering of Ga and Ge in the E2 position.

The valence electron count for $ReGa_2Ge$ is 17 e^- per formula unit. For this VEC, the $IrIn_3$-type compounds demonstrate semiconducting properties. Such "magic" VEC numbers are found not only in the $IrIn_3$ structure type, but also in other families of intermetallic compounds. For example, 18-electron half-Heusler and 24-electron full-Heusler compounds,[8−11] 14-electron Nowotny chimney-ladder phases,[12−14] 16-electron compounds of the $FeSi_2$ structure type,[55] and 12-electron compounds with the FeSi structure type[3,56] are all semiconductors. Deviations from the above VEC values usually lead to metallic properties, though some degree of tolerance within the certain range of VEC is observed, specific for a particular structure type.

Apparently, this scheme describes why the 16-electron $ReGa_3$ is formed under high-pressure conditions. Similar examples of compounds beyond the range of stability (in terms of VEC), which are formed under extreme (high-pressure) conditions, can be found in the family of Nowotny chimney-ladders. Specifically, the 15e^--Co_2Si_3 and 13.67e^--Mn_3Ge_5 are examples of high-pressure phases.[57,58]

As of now, there are no strict electron-counting rules, which could explain such behavior and/or predict it. However, there are emerging approaches applicable to some classes of compounds, for example, the 18−n rule[14] and its generalization as the 18−n + m rule.[59] This rule implies the tendency of a transition metal atoms to achieve a 18 e^- shell and thus explains the semiconducting ground state for a number of families of transition metal-based intermetallic compounds, although there are a number of violations.

The VEC of 17 for $ReGa_2Ge$ is also in accord with the 18−n rule. An analysis of the $IrIn_3$-type crystal structure provides the values of n and m (see Figure 1). Since there is a single chemical bond between transition metal atoms, the Re−Re dumbbell, an average number of electron pairs shared by each Re atom with neighboring same atoms is n = 1; there are no electrons that belong to bonding subsystems orthogonal to the Re-centered eigenfunctions (m = 0); therefore, the value of VEC = 18 − 1 = 17 indicates the stability of $ReGa_2Ge$ and anticipates its semiconducting properties.[59]

Unfortunately, the 18−n rule does not explain the appearance of stable 18-electron compounds within the $IrIn_3$ structure type, which are metallic conductors. In addition, it is worth noting that nonmetallic properties were predicted for the 15-electron compositions based on group 6 metals (TM_3, T = Cr, Mo, W and M = Ga, In),[60] although these compounds have not been synthesized so far. Therefore, the application and usefulness of the empirical 18−n rule remain ambiguous in certain cases and do not replace more direct ways of electronic structure and bonding analysis.

Electronic Structure. Structural parameters obtained from the single-crystal X-ray diffraction were used for electronic structure calculations. The calculations were carried out for Models A−C taking into account different options of gallium and germanium ordering in the E1 and E2 positions as described in the Experimental Section. Gallium and germanium were mixed in one position with the help of the virtual crystal approximation (VCA) using pseudoatoms with an intermediate charge (31.33 in Model A and 31.5 in Model C). This approach is easy to implement, since gallium and germanium are the fourth period neighbors. The calculated electronic structures near the Fermi level are presented in Figure 5 for all models.

The Models A, B, and C display qualitatively identical results. The calculations confirm the predicted semiconducting properties of $ReGa_2Ge$: for all models, the narrow energy gap is centered on the Fermi energy separating the valence and conduction bands. The band gap varies between 0.23 and 0.4 eV for Models A−C. This difference is insignificant and is consistent with typical discrepancies upon virtual atom approximation used in comparison with the ordered models.

All atoms contribute to the density of states near the Fermi level, but the contribution of rhenium states is much higher at the top of the valence band, while the bottom of the conduction band is primarily formed by the states of the p-elements. This is clearly seen in the calculated band structure (energy dispersion plot) presented in Figure 6 for Model A (calculated band structure plots for other models are given in Figure S2 of Supporting Information). The valence band maximum (VBM) formed by the Re 5d states is located at the Γ point of the Brillouin zone. The maxima close to the band gap at the R point and along the path of the k-vector from A to Z should be noted, too. These maxima are also formed predominantly by the rhenium states. On the contrary, the conduction band minimum (CBM) formed by the 4p states of E-atoms (mainly from the E2 sites) is located at the A point. It is important to mention that Models A and C give the same positions of VBM and CBM. For the ordered Model B, VBM and CBM are between A-Z and Z-Γ points, respectively. Therefore, all models show the mismatch of the top of the valence band and the bottom of the conduction band, which indicates an indirect band gap. From the electronic structure calculations, there is no evidence for anisotropic properties of $ReGa_2Ge$.

https://dx.doi.org/10.1021/acs.inorgchem.0c01805
Inorg. Chem. 2020, 59, 12748−12757

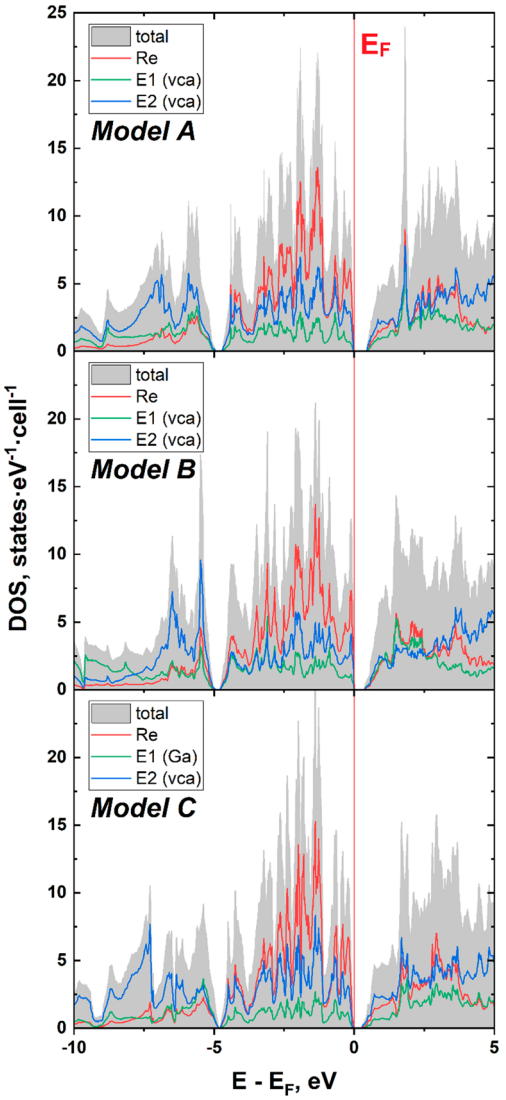

Figure 5. Calculated total and projected density of states near the Fermi level for $ReGa_2Ge$.

Thus, the electronic structure calculations confirm the empirical rule formulated for the $IrIn_3$ structure type[59] and predict the nonmetallic properties of $ReGa_2Ge$.

Chemical Bonding in $ReGa_2Ge$. More insight into the bonding scheme in $ReGa_2Ge$ is provided by the topological analysis of the electron localization function (ELF), which can offer information on three kinds of localization domains—atomic shells, lone pairs, and covalent bonds.

As seen from Figure 7, the structure of $ReGa_2Ge$ is a 3D network of covalent bonds. At high localization parameters, the domains corresponding to pairwise Re−Ge (Ω1) and Re−Ga (Ω2, Ω3) interactions are clearly observed, while at rather low η values one can see Re−Re interactions within dumbbells (Ω4). As the ELF features for $ReGa_2Ge$ cover a wide range from high to low localization parameter values, 2D ELF sections passing through the respective localization domains are also provided (Figure 8).

The integration of charge density within the bond basins Ω1-Ω4 gives the following basin populations: Ω1 (Re−Ge) − 1.45 e^-, Ω2 (Re−Ga) − 1.50 e^-, Ω3 (Re−Ga) − 1.11 e^-, and Ω4 (Re−Re) − 0.23 e^-. Thus, while the Re−E bonds at the distance of ca. 2.48 Å are not far from 2c-2 e^- bonds, and those at ca. 2.60 Å are slightly weaker and closer to 1 e^- bonds, the Re−Re interaction appears as a comparatively weaker covalent bond. This is in agreement with the corresponding distances of ca. 3 Å, which are measured almost exactly to the sum of covalent radii. No direct E−E bonds are observed, which is also consistent with long interatomic distances. This constitutes a major difference between bonding pattern for this compound and previously discovered phase with the same Re to E ratio, $ReGaGe_2$,[44] in which the Re−Ge and Re−Ga covalent bonds are accompanied by strong pairwise E−E interactions.

Calculated QTAIM Bader charges are −0.57 (Re), +0.05 (Ge), +0.26 (Ga), which confirms that the ionicity of the bonding in $ReGa_2Ge$ is rather low, with covalent interactions dominating the structure.

Transport Properties. Nonmetallic properties of $ReGa_2Ge$ were confirmed experimentally by the investigation of the temperature-dependent electrical resistivity, thermal conductivity, and Seebeck coefficient (Figure 9).

Electrical resistivity follows nonmetallic behavior; generally, it decreases with increasing the temperature. However, the resistivity at 250 K is only two times smaller than that at 2 K, and after passing a shallow minimum of 2.51×10^{-4} Ohm·m near 250 K, the resistivity slightly increases to 2.62×10^{-4} Ohm·m near 375 K. Linearization of the ln ρ versus $1/T$ plot is possible in the 50−200 K temperature range yielding a very narrow band gap, at least 1 order of magnitude smaller than the calculated gap. This discrepancy cannot be explained by a calculation error, since the methods based on DFT, as a rule, tend to underestimate a semiconducting band gap.

The observed $\rho(T)$ behavior of $ReGa_2Ge$ can be compared with the literature data. Other representatives of the $IrIn_3$ structure type also display a nonmonotonic temperature dependence of resistivity as well as a mismatch between the observed and calculated band gap.[15,61] For these compounds, the transfer of charge carriers across the band gap is observed at high temperatures, while the low-temperature resistivity is rationalized by the presence of in-gap states.[17] Thus, $FeGa_3$ obeys the Arrhenius law above 450 K,[61] Co- and Ni-doped $FeGa_3$ – above 650 K,[46] whereas for $OsGa_3$ this temperature is as high as 800 K.[17] Therefore, for $ReGa_2Ge$, the nonmonotonic dependence of resistivity at low temperatures (5−400 K) is likely a consequence of the complex real electronic structure in the vicinity of the Fermi energy due to the in-gap states, and activation mechanism should be observed at higher temperatures.

The Seebeck coefficient of $ReGa_2Ge$ is negative in the studied temperature range and decreases with increasing the temperature; however, the dependence is not monotonic. The temperature, at which a slight inflection is observed, correlates with the range of similar oscillations, clearly pronounced on the ln $\rho(1/T)$ dependence. The negative values of the Seebeck coefficient indicate that the main charge carriers are electrons. These data are also in agreement with the previously studied 17-electron compounds of the $IrIn_3$ structure type, for which similar results were obtained.[17] The absolute values of the Seebeck coefficient are about an order of magnitude higher than typical values for metals, which agrees well with nonmetallic properties of $ReGa_2Ge$.

The thermal conductivity, κ, of the sample is also in line with its semiconducting behavior. The temperature dependence of κ is typical for crystalline semiconductors.[62] Thermal conductivity reaches its maximum at low temperatures (~ 60 K) and then slightly decreases. The upturn above 300 K is most likely

https://dx.doi.org/10.1021/acs.inorgchem.0c01805
Inorg. Chem. 2020, 59, 12748−12757

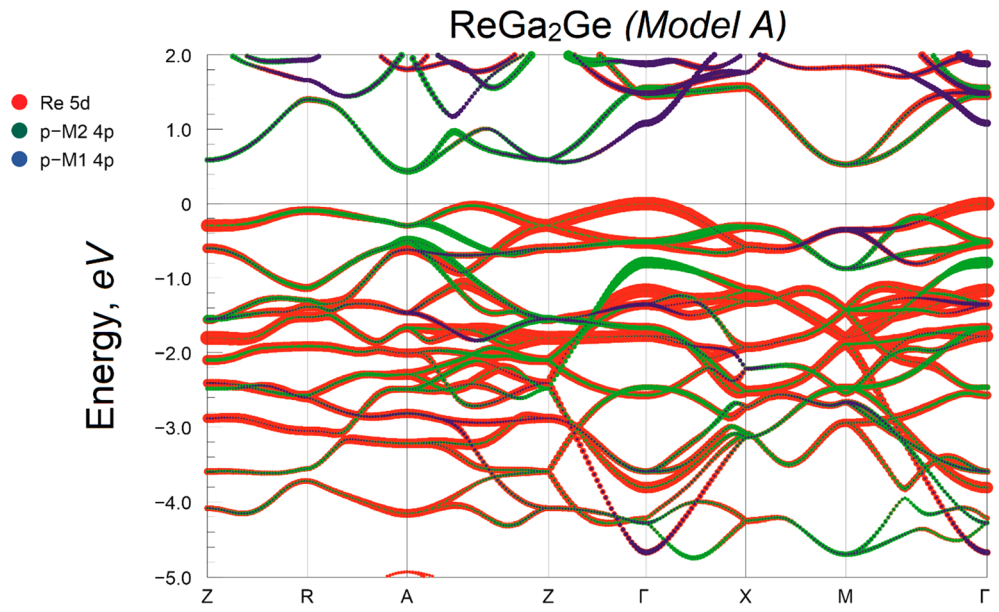

Figure 6. Band structure of $ReGa_2Ge$ near the Fermi level for Model A.

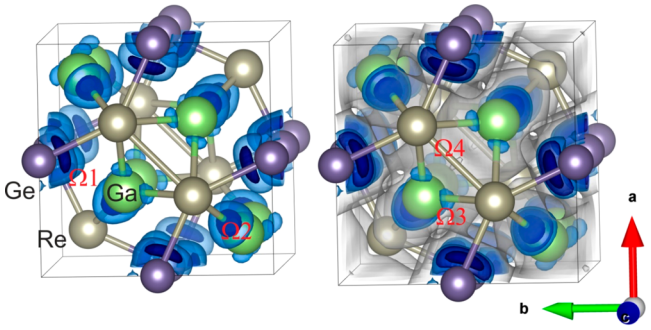

Figure 7. ELF isosurfaces for $ReGa_2Ge$ (Model B): dark blue – η = 0.84, blue – η = 0.78, light blue – η = 0.74, light gray – η = 0.47. For the explanation of Ω1–Ω4, see the text.

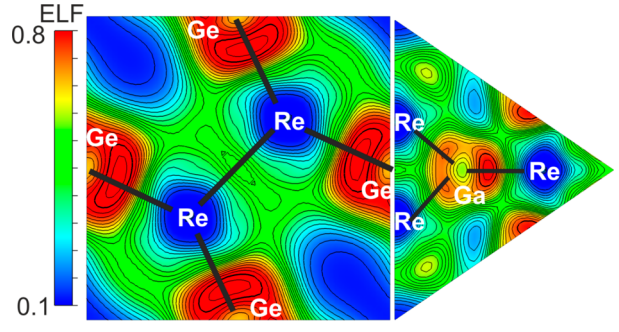

Figure 8. ELF cross sections passing through Re–Ge and Re–Re (left) and Re–Ga (right) interactions in $ReGa_2Ge$ (Model B).

associated with the radiation losses. The electronic contribution to the thermal conductivity, calculated according to the Wiedemann–Franz law as $\kappa_e = L_0 \cdot T/\rho$ (where L_0 = 2.45 × 10^{-8} W·Ohm·K^{-2} is the ideal Lorentz number), does not exceed 3.3%. In addition, the maximum value of κ, 1.5 W·m^{-1}·K^{-1}, is also in agreement with the nonmetallic properties. It is interesting to compare the thermal conductivity of $ReGa_2Ge$ and $FeGa_3$. The latter compound displays κ of about 7 W·m^{-1}·K^{-1},[17,45,63] which is almost five times greater than that for $ReGa_2Ge$. This difference is associated, on one hand, with a higher atomic mass of rhenium compared to iron, and, on the other hand, with the gallium and germanium incomplete ordering within the p-metal sublattice, which is also favorable for low lattice thermal conductivity. It should be noted that the maximum value of the calculated thermoelectric figure of merit ZT was 5 × 10^{-3} at 400 K.

CONCLUSIONS

A new ternary compound $ReGa_2Ge$ was synthesized as a single-phase polycrystalline sample, and its single crystals were grown in the temperature gradient of 750–700 °C using I_2 as a transport agent. $ReGa_2Ge$ crystallizes in the $IrIn_3$ structure type. Although gallium and germanium are the fourth period neighbors, no detectable homogeneity range was found for the title compound. The ^{69,71}Ga NQR spectroscopy study provides hints for at least partial ordering of gallium and germanium over the E1 and E2 positions, such that the E1 site is occupied solely by gallium, whereas the E2 position is statistically filled by both Ga and Ge. $ReGa_2Ge$ is predicted to be a semiconductor, which is typical for compounds of the $IrIn_3$ type with VEC = 17. The nonmetallic properties were confirmed both by the electronic structure calculations and from the temperature dependences of transport properties such as electrical resistivity, Seebeck coefficient, and thermal conductivity. Bonding analysis shows that covalent interactions dominate the structure, of which the Re–Ga and Re–Ge interactions are the strongest.

$ReGa_2Ge$ is the first representative of the $IrIn_3$ structure type that is based on the group 7 element and stable without application of external pressure, in contrast to a high-pressure phase $ReGa_3$. $ReGa_2Ge$ follows the empirical 18–n rule, as the aliovalent combination of Ga and Ge leads to the electron-precise value of VEC = 17. The replacement of each third gallium atom by a slightly smaller germanium atom induces chemical pressure in the crystal structure, which, in combination with the electronic factors, allows chemical stability of a compound to be achieved. This approach—the stabilization of phases that exist under extreme conditions by manipulating their composition and VEC can be used for the deliberate synthesis of new compounds with promising functional properties.

https://dx.doi.org/10.1021/acs.inorgchem.0c01805
Inorg. Chem. 2020, 59, 12748–12757

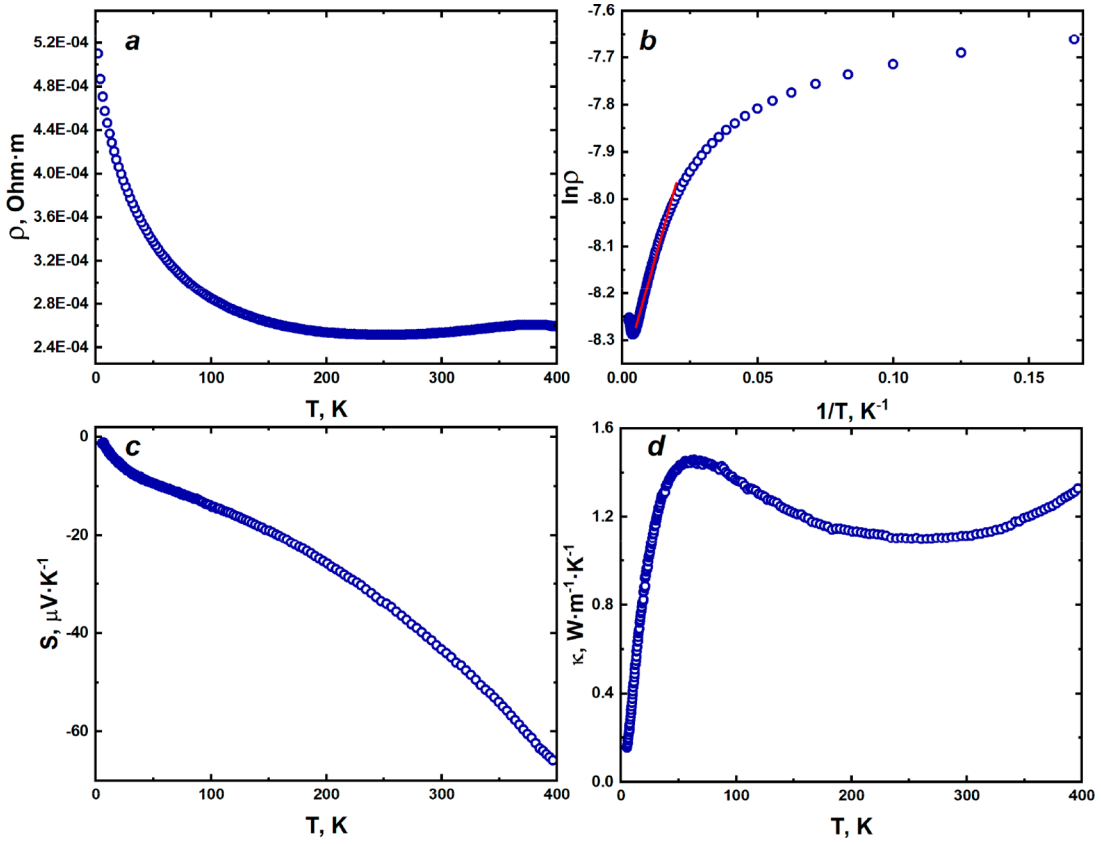

Figure 9. Electrical resistivity (a), and the corresponding ln ρ vs $1/T$ plot (b), Seebeck coefficient (c), and thermal conductivity (d) of $ReGa_2Ge$.

■ ASSOCIATED CONTENT

Supporting Information

The Supporting Information is available free of charge at https://pubs.acs.org/doi/10.1021/acs.inorgchem.0c01805.

Crystallographic and refinement parameters for the $ReGa_2Ge$ powder sample and its PXRD pattern, results of EDX analysis, and band structures of $ReGa_2Ge$ for Models B and C (PDF)

Accession Codes

CCDC 2008478−2008479 contain the supplementary crystallographic data for this paper. These data can be obtained free of charge via www.ccdc.cam.ac.uk/data_request/cif, or by emailing data_request@ccdc.cam.ac.uk, or by contacting The Cambridge Crystallographic Data Centre, 12 Union Road, Cambridge CB2 1EZ, UK; fax: +44 1223 336033.

■ AUTHOR INFORMATION

Corresponding Author

Andrei V. Shevelkov − *Department of Chemistry, Lomonosov Moscow State University, Moscow 119991, Russia;* orcid.org/0000-0002-8316-3280; Email: shev@inorg.chem.msu.ru

Authors

Maxim S. Likhanov − *Department of Chemistry, Lomonosov Moscow State University, Moscow 119991, Russia;* orcid.org/0000-0002-4683-8197

Valeriy Yu. Verchenko − *Department of Chemistry, Lomonosov Moscow State University, Moscow 119991, Russia; National Institute of Chemical Physics and Biophysics, Tallinn 12618, Estonia;* orcid.org/0000-0002-8000-425X

Andrei A. Gippius − *Department of Physics, Lomonosov Moscow State University, Moscow 119991, Russia; P.N. Lebedev Physics Institute RAS, Moscow 119991, Russia*

Sergei V. Zhurenko − *Department of Physics, Lomonosov Moscow State University, Moscow 119991, Russia; P.N. Lebedev Physics Institute RAS, Moscow 119991, Russia*

Alexey V. Tkachev − *P.N. Lebedev Physics Institute RAS, Moscow 119991, Russia*

Zheng Wei − *Department of Chemistry, University at Albany, SUNY, Albany, New York 12222, United States*

Evgeny V. Dikarev − *Department of Chemistry, University at Albany, SUNY, Albany, New York 12222, United States;* orcid.org/0000-0001-8979-7914

Alexey N. Kuznetsov − *Department of Chemistry, Lomonosov Moscow State University, Moscow 119991, Russia; N. S. Kurnakov Institute of General and Inorganic Chemistry RAS, Moscow 119991, Russia*

Complete contact information is available at: https://pubs.acs.org/10.1021/acs.inorgchem.0c01805

Notes

The authors declare no competing financial interest.

■ ACKNOWLEDGMENTS

We thank Dr. S. A. Vladimirova for carrying out DSC measurements. This work is supported by the Russian Science Foundation, Grant No. 19-73-00042. V.Yu.V. is grateful for the financial support from the Mobilitas program of the European Science Foundation, Grant No. MOBJD449. Z.W. and E.V.D. thank the National Science Foundation for supporting structural studies under Grant No. CHE-1955585. A.N.K. acknowledges

https://dx.doi.org/10.1021/acs.inorgchem.0c01805
Inorg. Chem. 2020, 59, 12748−12757

the support from the Presidium Program of Russian Academy of Sciences. The calculations were carried out partially using the equipment of the shared research facilities of the HPC computing resources at Lomonosov Moscow State University.

REFERENCES

(1) Steurer, W.; Dshemuchadse, J. *Intermetallics: Structures, Properties, and Statistics*; Oxford University Press: Oxford, UK, 2016.
(2) Oliynyk, A. O.; Mar, A. Discovery of intermetallic compounds from traditional to machine-learning approaches. *Acc. Chem. Res.* **2018**, *51*, 59−68.
(3) Tomczak, J. M. Thermoelectricity in correlated narrow-gap semiconductors. *J. Phys.: Condens. Matter* **2018**, *30*, 183001.
(4) Shevelkov, A. V. Chemical aspects of the design of thermoelectric materials. *Russ. Chem. Rev.* **2008**, *77*, 3−21.
(5) Buschow, K. H. J. The importance of ternary intermetallic compounds in science and technology. *J. Alloys Compd.* **1993**, *193*, 223−230.
(6) Carrete, J.; Mingo, N.; Wang, S.; Curtarolo, S. Nanograined Half-Heusler Semiconductors as Advanced Thermoelectrics: An Ab Initio High-Throughput Statistical Study. *Adv. Funct. Mater.* **2014**, *24*, 7427−7432.
(7) Sparks, T. D.; Gaultois, M. W.; Oliynyk, A. O.; Brgoch, J.; Meredig, B. Data mining our way to the next generation of thermoelectrics. *Scr. Mater.* **2016**, *111*, 10−15.
(8) Toboła, J.; Pierre, J.; Kaprzyk, S.; Skolozdra, R. V.; Kouacou, M. A. Crossover from semiconductor to magnetic metal in semi-Heusler phases as a function of valence electron concentration. *J. Phys.: Condens. Matter* **1998**, *10*, 1013−1032.
(9) Toboła, J.; Pierre, J. Electronic phase diagram of the XTZ (X = Fe, Co, Ni; T = Ti, V, Zr, Nb, Mn; Z = Sn, Sb) semi-Heusler compounds. *J. Alloys Compd.* **2000**, *296*, 243−252.
(10) Graf, T.; Felser, C.; Parkin, S. S. P. Simple rules for the understanding of Heusler compounds. *Prog. Solid State Chem.* **2011**, *39*, 1−50.
(11) Bende, D.; Wagner, F. R.; Grin, Yu. 8 − N rule and chemical bonding in main-group MgAgAs-type compounds. *Inorg. Chem.* **2015**, *54*, 3970−3978.
(12) Fredrickson, D. C.; Lee, S.; Hoffmann, R. The Nowotny chimney ladder phases: whence the 14 electron rule? *Inorg. Chem.* **2004**, *43*, 6159−6167.
(13) Fredrickson, D. C.; Lee, S.; Hoffmann, R.; Lin, J. The Nowotny chimney ladder phases: following the cpseudo clue toward an explanation of the 14 electron rule. *Inorg. Chem.* **2004**, *43*, 6151−6158.
(14) Yannello, V. J.; Fredrickson, D. C. Orbital origins of helices and magic electron counts in the Nowotny chimney ladders: the 18 − *n* rule and a path to incommensurability. *Inorg. Chem.* **2014**, *53*, 10627−10631.
(15) Häussermann, U.; Boström, M.; Viklund, P.; Rapp, Ö.; Björnängen, T. $FeGa_3$ and $RuGa_3$: semiconducting intermetallic compounds. *J. Solid State Chem.* **2002**, *165*, 94−99.
(16) Imai, Y.; Watanabe, A. Electronic structures of semiconducting $FeGa_3$, $RuGa_3$, $OsGa_3$, and $RuIn_3$ with the $CoGa_3$- or the $FeGa_3$-type structure. *Intermetallics* **2006**, *14*, 722−728.
(17) Amagai, Y.; Yamamoto, A.; Iida, T.; Takanashi, Y. Thermoelectric properties of semiconductorlike intermetallic compounds $TMGa_3$ (TM = Fe, Ru, and Os). *J. Appl. Phys.* **2004**, *96*, 5644−5648.
(18) Takagiwa, Y.; Kitahara, K.; Matsubayashi, Y.; Kimura, K. Thermoelectric properties of FeGa3-type narrow-bandgap intermetallic compounds $Ru(Ga,In)_3$: experimental and calculational studies. *J. Appl. Phys.* **2012**, *111*, 123707.
(19) Haldolaarachchige, N.; Phelan, W. A.; Xiong, Y. M.; Jin, R.; Chan, J. Y.; Stadler, S.; Young, P. Thermoelectric properties of intermetallic semiconducting $RuIn_3$ and metallic $IrIn_3$. *J. Appl. Phys.* **2013**, *113*, No. 083709.
(20) Kitahara, K.; Takagiwa, Y.; Kimura, K. Unified cluster-based description of valence bands in AlIr, $RuAl_2$, $RuGa_3$ and Al-TM quasicrystalline approximants. *J. Phys.: Conf. Ser.* **2017**, *809*, No. 012014.
(21) Viklund, P.; Lidin, S.; Berastegui, P.; Häussermann, U. Variations of the $FeGa_3$ structure type in the systems $CoIn_{3-x}Zn_x$ and $CoGa_{3-x}Zn_x$. *J. Solid State Chem.* **2002**, *165*, 100−110.
(22) Pottgen, R.; Hoffmann, R.-D.; Kotzyba, G. Structure, chemical bonding, and properties of $CoIn_3$, $RhIn_3$, and $IrIn_3$. *Z. Anorg. Allg. Chem.* **1998**, *624*, 244−250.
(23) Popova, S. V.; Fomicheva, L. N. New phases in Re-Ga and Os-Ga systems, obtained at a high pressure. *Inorg. Mater.* **1982**, *18*, 205−208.
(24) Clark, W. G.; Hanson, M. E.; Lefloch, F.; Ségransan, P. Magnetic resonance spectral reconstruction using frequency-shifted and summed Fourier transform processing. *Rev. Sci. Instrum.* **1995**, *66*, 2453.
(25) *SAINT*, Version 8.38A; Bruker AXS Inc.: Madison, Wisconsin, USA, 2017.
(26) Krause, L.; Herbst-Irmer, R.; Sheldrick, G. M.; Stalke, D. Comparison of Silver and Molybdenum Microfocus X-ray Sources for Single-crystal Structure Determination. *J. Appl. Crystallogr.* **2015**, *48*, 3−10.
(27) *SADABS*, v. 2014/5; Bruker AXS Inc.: Madison, WI, 2015.
(28) Petricek, V.; Dusek, M.; Palatinus, L. Crystallographic computing system JANA2006: general features. *Z. Kristallogr. - Cryst. Mater.* **2014**, *229*, 345−352.
(29) Koepernik, K.; Eschrig, H. Full-Potential Nonorthogonal Local-Orbital Minimum-Basis Band-Structure Scheme. *Phys. Rev. B: Condens. Matter Mater. Phys.* **1999**, *59*, 1743.
(30) Perdew, J. P.; Wang, Y. Accurate and Simple Analytic Representation of the Electron-Gas Correlation Energy. *Phys. Rev. B: Condens. Matter Mater. Phys.* **1992**, *45*, 13244.
(31) Blöchl, P. E.; Jepsen, O.; Andersen, O. K. Improved Tetrahedron Method for Brillouin-Zone Integrations. *Phys. Rev. B: Condens. Matter Mater. Phys.* **1994**, *49*, 16223.
(32) Kresse, G.; Joubert, D. From ultrasoft pseudopotentials to the projector augmented-wave method. *Phys. Rev. B: Condens. Matter Mater. Phys.* **1999**, *59*, 1758−1775.
(33) Kresse, G.; Furthmüller, J. Vienna Ab initio Simulation Package (VASP), v.5.4.4, http://www.vasp.at/.
(34) Perdew, J. P.; Burke, K.; Ernzerhof, M. Generalized Gradient Approximation Made Simple. *Phys. Rev. Lett.* **1996**, *77*, 3865−3868.
(35) Monkhorst, H. J.; Pack, J. D. Special points for Brillouin-zone integrations. *Phys. Rev. B* **1976**, *13*, 5188−5192.
(36) Lu, T.; Chen, F. Multiwfn: A multifunctional wavefunction analyzer. *J. Comput. Chem.* **2012**, *33*, 580−592.
(37) Momma, K.; Izumi, F. VESTA 3 for three-dimensional visualization of crystal, volumetric and morphology data. *J. Appl. Crystallogr.* **2011**, *44*, 1272−1276.
(38) Siegrist, T.; Hulliger, F.; Petter, W. The crystal structure of Re_3Ge_7. *J. Less-Common Met.* **1983**, *90*, 143−151.
(39) Xie, W.; Luo, H.; Phelan, B. F.; Klimczuk, T.; Cevallos, F. A.; Cava, R. J. Endohedral gallide cluster superconductors and superconductivity in $ReGa_5$. *Proc. Natl. Acad. Sci. U. S. A.* **2015**, *112*, E7048−E7054.
(40) Likhanov, M. S.; Verchenko, V. Yu.; Kuznetsov, A. N.; Shevelkov, A. V. $ReGa_{0.4}Ge_{0.6}$: Intermetallic compound with pronounced covalency in the bonding pattern. *Inorg. Chem.* **2019**, *58*, 2822−2832.
(41) Pöttgen, R. Preparation, crystal structure and properties of $RuIn_3$. *J. Alloys Compd.* **1995**, *226*, 59−64.
(42) Korolkov, I. V.; Gubanov, A. I.; Gromilov, S. A. Thermolysis of $[Pt(NH_3)_4][ReHlg_6]$ (Hlg = Cl, Br). Structure refinement for $[Pt(NH_3)_4][ReCl_6]$. *J. Struct. Chem.* **2005**, *46*, 479−487.
(43) Umeo, K.; Hadano, Y.; Narazu, S.; Onimaru, T.; Avila, M. A.; Takabatake, T. Ferromagnetic instability in a doped band gap semiconductor $FeGa_3$. *Phys. Rev. B: Condens. Matter Mater. Phys.* **2012**, *86*, 144421.
(44) Likhanov, M. S.; Khalaniya, R. A.; Verchenko, V. Yu.; Gippius, A. A.; Zhurenko, S. V.; Tkachev, A. V.; Fazlizhanova, D. I.; Kuznetsov, A. N.; Shevelkov, A. V. $ReGaGe_2$: an intermetallic compound with semiconducting properties and localized bonding. *Chem. Commun.* **2019**, *55*, 5821−5824.

https://dx.doi.org/10.1021/acs.inorgchem.0c01805
Inorg. Chem. 2020, 59, 12748−12757

(45) Wagner-Reetz, M.; Cardoso-Gil, R.; Grin, Y. Substitution solid solutions $FeGa_{3-x}E_x$ and their thermoelectric properties. *J. Electron. Mater.* **2014**, *43*, 1857−1864.
(46) Likhanov, M. S.; Verchenko, V. Yu.; Bykov, M. A.; Tsirlin, A. A.; Gippius, A. A.; Berthebaud, D.; Maignan, A.; Shevelkov, A. V. Crystal growth, electronic structure, and properties of Ni-substituted $FeGa_3$. *J. Solid State Chem.* **2016**, *236*, 166−172.
(47) Gamza, M. B.; Tomczak, J. M.; Brown, C.; Puri, A.; Kotliar, G.; Aronson, M. C. Electronic correlations in $FeGa_3$ and the effect of hole doping on its magnetic properties. *Phys. Rev. B: Condens. Matter Mater. Phys.* **2014**, *89*, 195102.
(48) Likhanov, M. S.; Zhupanov, V. O.; Verchenko, V. Yu.; Gippius, A. A.; Zhurenko, S. V.; Tkachev, A. V.; Fazlizhanova, D. I.; Berthebaud, D.; Shevelkov, A. V. Synthesis, extended and local crystal structure, and thermoelectric properties of $Fe_{1-x}Re_xGa_3$ solid solution. *J. Alloys Compd.* **2019**, *804*, 331−338.
(49) Wagner, M.; Cardoso-Gil, R.; Oeschler, N.; Rosner, H.; Grin, Yu. $RuIn_{3-x}Sn_x$, $RuIn_{3-x}Zn_x$, and $Ru_{1-y}In_3$ − new thermoelectrics based on the semiconductor $RuIn_3$. *J. Mater. Res.* **2011**, *26*, 1886−1893.
(50) Kasinathan, D.; Wagner, M.; Koepernik, K.; Cardoso-Gil, R.; Grin, Yu.; Rosner, H. Electronic and thermoelectric properties of $RuIn_{3-x}A_x$ (A = Sn, Zn). *Phys. Rev. B: Condens. Matter Mater. Phys.* **2012**, *85*, No. 035207.
(51) Verchenko, V. Yu.; Zubtsovskii, A. O.; Tsirlin, A. A.; Shevelkov, A. V. Chemical pressure in the correlated narrow-gap semiconductor $FeGa_3$. *J. Mater. Sci.* **2019**, *54*, 2371−2378.
(52) Hlukhyy, V.; Hoffmann, R.-D.; Pöttgen, R. The Solid Solution $Mg_xIn_{3-x}Ir$ − Formation of the $FeGa_3$ Type up to x = 0.73 and the Cementite Structure with x = 0.92. *Z. Anorg. Allg. Chem.* **2004**, *630*, 68−74.
(53) Verchenko, V. Yu.; Likhanov, M. S.; Kirsanova, M. A.; Gippius, A. A.; Tkachev, A. V.; Gervits, N. E.; Galeeva, A. V.; Büttgen, N.; Krätschmer, W.; Lue, C. S.; Okhotnikov, K. S.; Shevelkov, A. V. Intermetallic solid solution $Fe_{1-x}Co_xGa_3$: Synthesis, structure, NQR study and electronic band structure calculations. *J. Solid State Chem.* **2012**, *194*, 361−368.
(54) Gippius, A. A.; Verchenko, V. Yu.; Tkachev, A. V.; Gervits, N. E.; Lue, C. S.; Tsirlin, A. A.; Büttgen, N.; Krätschmer, W.; Baenitz, M.; Shatruk, M.; Shevelkov, A. V. Interplay between localized and itinerant magnetism in Co-substituted $FeGa_3$. *Phys. Rev. B: Condens. Matter Mater. Phys.* **2014**, *89*, 104426.
(55) Du, X.; Hu, P.; Mao, T.; Song, Q.; Qiu, P.; Shi, X.; Chen, L. Ru Alloying Induced Enhanced Thermoelectric Performance in $FeSi_2$-Based Compounds. *ACS Appl. Mater. Interfaces* **2019**, *11*, 32151−32158.
(56) Pshenay-Severin, D. A.; Burkov, A. T. Electronic Structure of B20 (FeSi-Type) Transition-Metal Monosilicides. *Materials* **2019**, *12*, 2710.
(57) Larchev, V. I.; Popova, S. V. The new chimney ladder phases Co_2Si_3 and Re_4Ge_7 formed by treatment at high temperatures and pressures. *J. Less-Common Met.* **1982**, *84*, 87−91.
(58) Takizawa, H.; Sato, T.; Endo, T.; Shimada, M. High-Pressure synthesis and electrical properties of Mn_3Ge_5 with $Mn_{11}Si_{19}$-type structure. *J. Solid State Chem.* **1987**, *68*, 234−238.
(59) Yannello, V. J.; Fredrickson, D. C. Generality of the 18−*n* rule: intermetallic structural chemistry explained through isolobal analogies to transition metal complexes. *Inorg. Chem.* **2015**, *54*, 11385−11398.
(60) Boucher, B.; Al Rahal Al Orabi, R.; Fontaine, B.; Grin, Yu.; Gautier, R.; Halet, J.-F. Enhancement of the thermoelectric properties of $FeGa_3$-type structures with group 6 transition metals: a computational exploration. *Inorg. Chem.* **2017**, *56*, 4229−4237.
(61) Hadano, Y.; Narazu, S.; Avila, M. A.; Onimaru, T.; Takabatake, T. Thermoelectric and Magnetic Properties of a Narrow-Gap Semiconductor $FeGa_3$. *J. Phys. Soc. Jpn.* **2009**, *78*, No. 013702.
(62) White, M. A. *Properties of Materials*; Oxford University Press: New York, Oxford, 1999.
(63) Takagiwa, Y.; Matsuura, Y.; Kimura, K. Effect of Carrier-Doping on the Thermoelectric Properties of Narrow-Bandgap $(Fe,Ru)Ga_3$ Intermetallic Compounds. *J. Electron. Mater.* **2014**, *43*, 2206−2211.

https://dx.doi.org/10.1021/acs.inorgchem.0c01805
Inorg. Chem. 2020, 59, 12748−12757